Feasibility of measuring thermoelectric potentials over self-assembled monolayers with C-AFM

THESIS

submitted in partial fulfillment of the
requirements for the degree of

MASTERS
in
PHYSICS

Author :	M.L. Pleijster
Student ID :	1319582
Supervisor :	Dr. S.J. van der Molen
Daily supervisor:	Drs. H. Ateşçi
2nd corrector :	Dr. I.M.N. Groot

Leiden, The Netherlands, May 1, 2015

Feasibility of measuring thermoelectric potentials over self-assembled monolayers with C-AFM

M.L. Pleijster

Huygens-Kamerlingh Onnes Laboratory, Leiden University
P.O. Box 9500, 2300 RA Leiden, The Netherlands

May 1, 2015

Abstract

Combining an applied thermal potential with Conductive Atomic Force Microscopy (C-AFM) enables the measurement of thermoelectric properties of Self-Assembled Monolayers (SAM). Such measurements can be used to show the presence of destructive quantum interference in molecules. To study the feasibility of measuring thermoelectric potentials over SAMs with C-AFM, we have simulated the temperature distribution around the tip in a typical C-AFM setup with finite element simulations in Comsol. These show that a sufficiently large temperature difference can develop across the molecular layer to measure the thermoelectric properties.

Contents

1   Introduction

Molecular electronics provides great potential for a cheap and easy bottom-up approach to fabricate electronics. This could be used in ways that are not possible with traditional silicon based technologies. Single molecule electronics carries the promise to extend Moore's law to the fundamental limit of a single transistor per molecule. Even if this goal is never attained, the development of organic electronics enables the fabrication of extremely innovative products that are otherwise unavailable. Due to the bottom-up approach of Molecular Electronics, functional molecules can be designed with specific properties by altering the chemistry. This makes for an exciting field of research.

Much of the research in Molecular Electronics is therefore devoted to discovering and designing molecular structures with interesting electrical properties. To measure these properties scanning probe microscopy techniques are often used. Scanning Tunneling Microscopy (STM) is a technique to probe the conductivity of both single and aggregated molecules[1, 2]. Another common technique is Conductive Atomic Force Microscopy (C-AFM). Although this method is less suitable for measurements on single molecules due to the larger size of an AFM-tip than an STM-tip. C-AFMs are well suited for the study of molecular self assembled monolayers (SAMs)[3, 4].

Most measurements revolve around determining the conductance of single or aggregated molecules. In this report we will discuss the possibility of retrieving more information about the molecule by measuring the thermoelectric properties of the molecule. In particular, measuring a thermoelectric potential over a molecular layer and by that method determine its Seebeck coefficient. This can reveal information about the electronic transport properties of the molecular junction, which are often expressed in terms of a Transmission Function $T(E)$. This information is not available from conductance measurements.

We want to do this by applying the molecular layer onto a gold substrate and approach it with an AFM tip. By heating one side of this junction, we want to create the temperature difference that gives rise to the thermoelectric potential. However the thermal potential that we get over the layer of molecules is not just the temperature difference we get by heating. In general it will be less, because some heat will be transferred between the substrate and the tip. Either directly via thermal conduction through the molecular layer or via radiation and convection through the surrounding air. In this study we attempt to quantify this, by modelling the geometry of our setup and its heat transfer properties with a finite el-

ement simulation in the commercial program of Comsol Multiphysics[5].

Furthermore we will discuss the feasibility of using these type of thermopower measurements as a method to show the existence of destructive quantum interference in certain molecules. The existence of which has only been demonstrated indirectly with conductance measurements[3, 6, 7] and thermopower measurements could provide a second independent proof. We will also go into the practical design considerations for modifying an existing C-AFM setup to enable this type of measurements. We will show some of the challenges faced when attempting this and provide some pointers to avoid potential pitfalls.

In this report we will not show any new thermopower measurements on molecular junctions, but focus on whether or not this type of experiment is fundamentally possible. As SAMs are only nanometers in depth, it is questionable if any significant temperature difference can exist between two points that are so close together. Simulations in Comsol are used to determine if it is possible to generate a sufficiently large temperature difference across the molecular junction. They are also used to determine under what conditions such a potential can be used to accurately measure the thermoelectric properties of a molecular junction.

2 Theory of Molecular Conductance and Thermoelectricity

In the field of molecular electronics we are mostly interested in the conductive properties of single or multiple molecules between two electrodes. Common techniques involve the use of scanning probe microscopy, such as STM and AFM, and the use of Mechanically Controlled Break Junctions (MCBJ). This report focuses mostly on the former. However, most of the underlying physics is very similar, so the following theory can be applied to both techniques.

2.1 Ballistic Transport

If the mean free path of an electron is much larger than the dimensions of the medium, a medium can be said to display ballistic transport. For small molecules and atomic chains this is often a good model to describe charge transport. In particular, if we assume a 1D conductor on the nanoscale attached to two electrodes and we apply a bias voltage V_b, we can deduce from this model that the current through this 1D conductor is given by[8, 9]:

$$I = \frac{2e}{2\pi} \int_{-\infty}^{\infty} v(E)g(E) \left(f_L(E) - f_R(E) \right) \mathrm{dE} \qquad (1)$$

$$= \frac{2e^2}{h} V_b. \qquad (2)$$

Here $v(E) = \sqrt{2E/m}$ is the velocity of an electron travelling through the conductor with energy E and $g(E) = \frac{1}{\hbar}\sqrt{\frac{m}{2E}}$ is the density of states of the conductor corresponding to running wave solutions[10]. The applied bias shifts the chemical potentials in such a way that $\mu_L - \mu_R = eV_b$, determining the Fermi-Dirac functions in the left and right leads:

$$f_{L,R}(E) = \left(1 + \exp\left(\frac{E - \mu_{L,R}}{k_B T} \right) \right)^{-1}. \qquad (3)$$

In metals, electrical resistance is usually attributed to phonon scattering for high temperatures[10]. In the ballistic regime the mean free path is much larger than the dimensions of the medium, so we assume that no such scattering events take place. A ballistic conductor should therefore be a 'perfect' conductor without resistance. The quantum mechanical nature of our electrodes makes that equation 1 integrates to a finite conductance of $G_0 = \frac{2e^2}{h}$, corresponding to a resistance of $R_0 \approx 12.9k\Omega$. This

finite resistance should be associated with resistance arising at the interfaces between the electrodes and the ballistic conductor[11]. The value G_0 is a fundamental constant and is commonly referred to as the quantum of conductance. It was first observed in a two dimensional electron gas (2DEG) by tuning the width of the channels with electrostatic gates[12].

So far, we are assuming that we have a perfect conductor and that all electrons with energies in the bias window contribute equally to the current and can pass through the conductor. We can extend this model by introducing a scattering probability $R(E)$ denoting the chance for an electron with energy E to be reflected back into the source electrode. We also define the transmission probability $T(E) = 1 - R(E)$. When we incorporate this transmission probability in our model of equation 1 and we cancel the common terms in the group velocity and the density of states this leads to:

$$I = \frac{2e}{h} \int_{-\infty}^{\infty} T(E) \left(f_L - f_R\right) \mathrm{dE}. \tag{4}$$

This result is known as the Landauer-Büttiker Formalism and is in fact much more general than the simple quantum ballistic model we have used so far[13]. Later we will try to make this more rigorous by doing a fully quantum mechanical treatment of the scattering formalism, but first we will have a look at the implications and meaning of the Landauer-Büttiker formula.

2.2 The Transmission Function $T(E)$

The transmission probability $T(E)$ for an electron with energy E is commonly called the transmission function. The Landauer-Büttiker formalism from equation 4 shows that knowing the transmission function is sufficient to determine the current through a conductor.

The energy levels corresponding to the running wave solutions for the electrons moving through the ballistic conductor are given by[10]:

$$E = \frac{\hbar^2}{2m} k^2 = \frac{\hbar^2}{2m} \left(\frac{2\pi n}{L}\right)^2, \tag{5}$$

with n an integer. Molecules have sizes in the order of nanometers, thus the energy spacings are very large according to equation 5. For low bias voltages we can assume that there is only one energy level within the transport window. This single level corresponds to either the Highest Occupied Molecular Orbital (HOMO) or the Lowest Unoccupied Molecular Orbital (LUMO) of the molecule, depending on which energy level

is closer to the Fermi energy of the metal electrodes. Although there is a priori no way to determine which level is the closest, because the coupling of the molecule to the electrodes shifts the energy levels of the molecules with respect to the vacuum energy.

Another consequence of the coupling between a molecule and the electrodes is that, instead of a well defined molecular energy level, the energy level broadens. This is due to the uncertainty principle $\Delta E \Delta t \geq \hbar$, since an electron no longer permanently resides on the molecule, but is only on the molecule for a finite time. This broadening of the energy spectrum can be represented by a Lorentzian function[14, 15]:

$$T(E) = \frac{\Gamma^2}{(E - \epsilon)^2 + \Gamma^2/4}.$$ (6)

The factor Γ denotes the amount of coupling to the leads, which in this case is chosen to be symmetric. The Lorentzian is centered around the molecular energy level ϵ. Figure 1a shows a Lorentzian centered around $\epsilon = 2$eV. The corresponding IV-curve is displayed in 1b and shows steps in the current when the energy of the applied bias equals twice the molecular energy level:

$$eV_b = 2\epsilon.$$ (7)

Due to the symmetric coupling to the leads in this example, the steps occur at 2ϵ and also explain the symmetry of the graph.

2.3 Tight Binding

Using the ballistic transport model we have gained a better intuition for molecular conductance. In particular we have tried to show the importance of the Transmission function $T(E)$. We would now like to provide an alternative view to the ballistic model, because molecular conductors are not always best described as a material were the electrons can flow through freely from one electrode to the other. We have already hinted that many of the results we got from the ballistic approach are valid in a more general way. In fact the formal treatment of the tight binding model is quite similar to that of ballistic transport if we make use of Scattering matrices and Green's functions[16]. However, in this section I will only present a basic tight binding model, so that we have a better understanding of the underlying physics when the description by the ballistic model is insufficient.

Within the molecule, electrons will reside in the states formed by the different molecular orbitals. In order for such a state to contribute to the

(a)   **(b)**
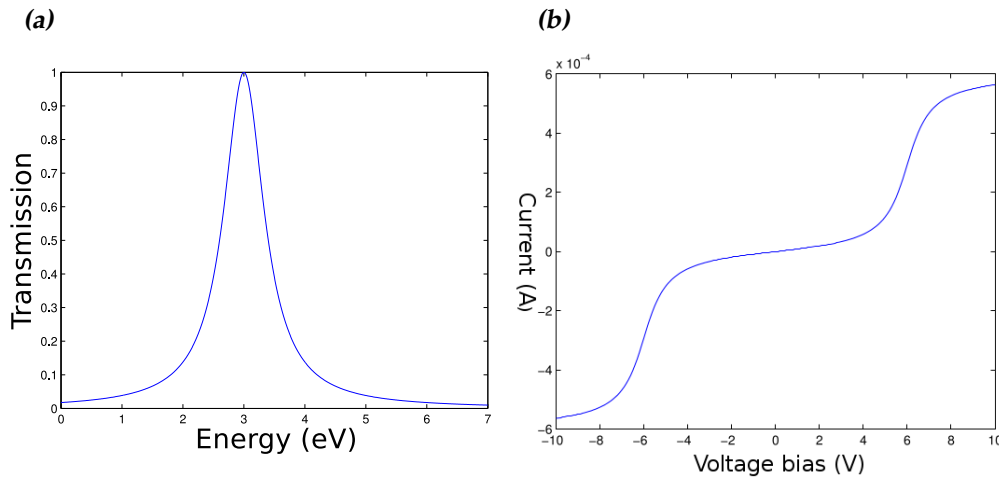
Figure 1: *A Lorentzian Transmission function $T(E)$ (a) as a function of energy and the current-voltage characteristics derived from it (b) is shown as a function of electrode potential. Note that the applied bias is symmetric over the electrodes and thus a step in the current occurs at twice the energy of the Lorentzian energy level ϵ.*

conductance, its energy must be accessible for the electrons from the leads. The tight binding model assumes that these electrons are temporarily residing in the molecular orbitals. As there is some overlap between these orbitals, state transitions can occur with a transition energy denoted by the hopping parameter α[1]. For some simple linear molecule we can imagine this schematically as in figure 2a. Here the ϵ_0's denote two localized orbitals and the probability for a transition from one state to the neighbouring state is taken to be α. The left- and right energy levels are coupled to the electrodes on either side with a coupling factor $\gamma_{L,R}$. These interactions can be represented by a Hamiltonian for the isolated molecule with two levels at energy ϵ_0 as:

$$\mathbf{H}_{mol} = \begin{pmatrix} \epsilon_0 & \alpha \\ \alpha & \epsilon_0 \end{pmatrix}. \tag{8}$$

This Hamiltonian can be used to calculate the Transmission function $T(E)$ by using Non-equilibrium Green's functions (NEGF). In the next section we will demonstrate this technique by calculating the transmission function $T(E)$ for this model and for a three sites model displaying quantum interference in the conductance. For the moment we will state that the

---

[1]In cases with a single hopping parameter the parameter is often denoted with a t.

Transmission Function $T(E)$ for the tight binding model with two levels is given by:

$$T(E) \approx \gamma^2 \left| \frac{\alpha}{(E - \epsilon_0)^2} \right|^2, \tag{9}$$

for energies far away from the the molecular energy level. In this calculation we have also assumed that the coupling factor to the electrodes does not depend on energy and set $\Gamma = \gamma$. Thus this equation is similar to equation 6 when $E - \epsilon_0 >> \Gamma$.
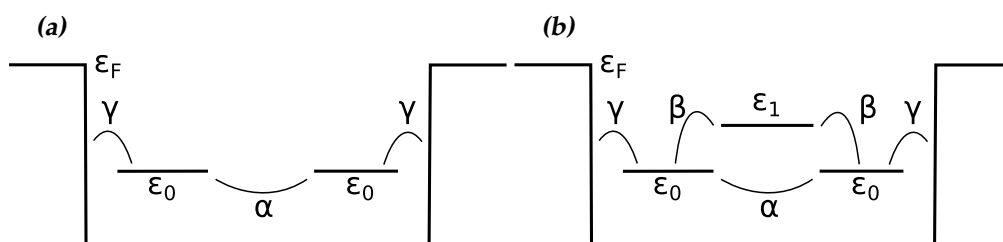
Figure 2: *Two Tight Binding models: (a) A simple linear model for Tight Binding. The two orbitals are denoted with their energy ϵ_0. There is a uniform hopping parameter α. The coupling to the electrodes is symmetric and denoted by the constant γ. (b) The three sites model has an orbital at a different energy ϵ_1, due to this there is now an upper and a lower path to get from the left electrode to the right. The hopping parameter between the two lower energy levels is given by α, while the parameter to go between ϵ_0 and ϵ_1 is denoted by β..*

2.4   Destructive Quantum Interference

Molecular conductors are, due to their nano-scale sizes, governed by quantum effects. One interesting effect is quantum interference in the conductance. This effect could be used for molecular devices to switch or tune their conductance by chemistry[17]. A simple explanation of quantum interference in a molecular conductor is given by the three sites model, which we will detail below.

In the simple linear molecule with two localized molecular orbitals, that we discussed before, there will be no quantum interference. The molecule AC-DT has two such orbitals, which are schematically shown in figure 3b and thus does not display destructive quantum interference, as can be seen in the Transmission function $T(E)$ for AC-DT in figure 3a which has been calculated by Troels Markussen and Kristian S. Thygesen

by using Non-Equilibrium Green's Functions (NEGF) methods combined with a DFT+Σ calculation for the orbitals[17].[2]Here we see that for the AC-DT molecule the transmission has peaks on the logarithmic scale, when the electron energy E matches that of the orbital ϵ, where the peak can be best described by the Lorentzian function of equation 6. There is still a relatively high probability for an electron with energy E that doesn't corresponds to the energy of the orbital to be transmitted. This is described by the result for the simpler tight-binding model, we got in equation 9.

When there is a third orbital, destructive quantum interference could occur. In the three sites model we assume that an electron coming from the leads can not directly transfer into this orbital, but that this additional energy level provides an extra path for the electron to go from the left to the right, as is shown in figure 3d for the molecule AQ-DT. The phase of the electron travelling through this second path can be different from that of an electron that doesn't travel through this extra orbital. When the phase difference between these two paths is equal two π destructive quantum interference occurs. The calculation of the Transmission function $T(E)$ for the AQ-DT molecule displays strong destructive quantum interference at an energy of about 0.75eV above the Fermi energy. This is displayed in figure 3a and the contributions to the Transmission Function of the different paths is shown in 3c.

To have a better understanding of quantum interference we will calculate the Transmission function $T(E)$ for the simple three sites model using Equilibrium Green's Functions (EGF). Since a full treatment of EGF is outside the scope of this text, we state that the Transmission function is related to Green's functions by[8]:

$$T(E) = \text{Tr}\left[\mathbf{\Gamma}_L \mathbf{G}^r(E) \mathbf{\Gamma}_R \mathbf{G}^a(E)\right]. \tag{10}$$

For a Hamiltonian $\mathbf{H}$ the advanced and retarded Green's functions are defined by:

$$\mathbf{G}^{r,a}(E) = \lim_{\eta \to 0}\left[(E \pm i\eta)\mathbf{I} - \mathbf{H}\right]^{-1}. \tag{11}$$

Here $\mathbf{I}$ denotes the identity operator. The imaginary infinitesimal energy $\pm i\eta$ selects between the advanced or forward in time solution and the retarded or time-reversed. For the three sites model we can define the coupling matrices $\mathbf{\Gamma}_{L,R}$ as:

$$\mathbf{\Gamma}_L = \begin{pmatrix} \gamma & 0 & 0 \\ 0 & 0 & 0 \\ 0 & 0 & 0 \end{pmatrix}, \mathbf{\Gamma}_R = \begin{pmatrix} 0 & 0 & 0 \\ 0 & \gamma & 0 \\ 0 & 0 & 0 \end{pmatrix}, \tag{12}$$

---

[2]For details on the method of a DFT+Σ calculation see reference [17].
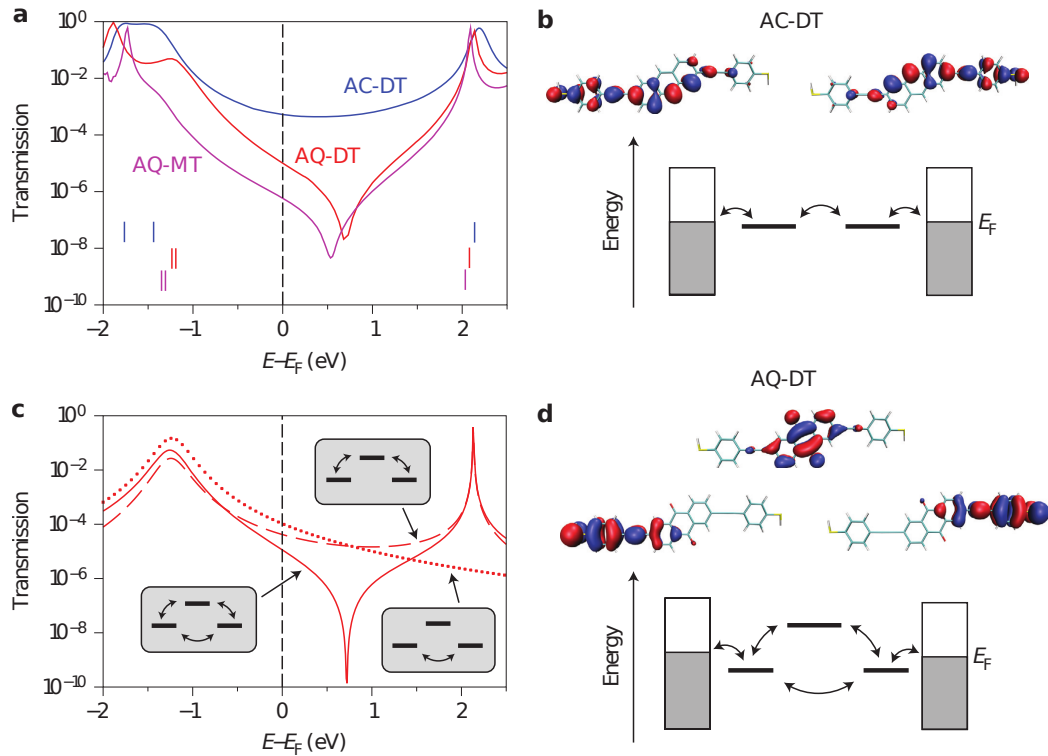
Figure 3: *Calculations done by Troels Markussen and Kristian S. Thygesen [17] show the Transmission function $T(E)$ for the molecules AC-DT, AQ-DT and AQ-MT in (a). The orbitals and energy levels are shown in (b) and (d). While the contributions to the Transmission function $T(E)$ of the different paths are shown in (c) for AQ-DT. In the transmission function for AQ-DT and AQ-MT a strong dip is visible denoting destructive quantum interference in the conduction. This is not present for the AC-DT molecule.*

because only the left and right orbitals couple to the electrodes. Here we also use the wide band limit approximation and assume that the coupling strength is the same for all energies. Applying these coupling matrices to equation 10 we find that of the Green's function $\mathbf{G}(E)$, the only matrix element of interest is the element G_{12}, which corresponds to the electron transport from the left electrode to the right. This leads to the Transmission function:

$$T(E) = \gamma^2 |G_{12}|^2. \tag{13}$$

When we look at off-resonance transport, for which $E - \epsilon_0 >> \gamma$, we can write the three sites Hamiltonian as a matrix of energies $\epsilon_{0,1}$ and coupling

factors between the levels α, β as indicated in figure 2b:

$$\mathbf{H} = \begin{pmatrix} \epsilon_0 & \alpha & \beta \\ \alpha & \epsilon_0 & \beta \\ \beta & \beta & \epsilon_1 \end{pmatrix}. \tag{14}$$

Using this Hamiltonian in equation 11 to calculate the corresponding Green's function, we get[3]

$$\mathbf{G}(E) = \begin{pmatrix} E - \epsilon_0 & -\alpha & -\beta \\ -\alpha & E - \epsilon_0 & -\beta \\ -\beta & -\beta & E - \epsilon_1 \end{pmatrix}^{-1}. \tag{15}$$

We could solve this directly to find the Transmission function, but it is more insightful to treat the upper and lower paths separately. For the lower route we set the perturbation $\beta = 0$. For the upper route we set $\alpha = 0$. For the lower route $\mathbf{G}^{lower}$ reduces to:

$$\mathbf{G}^{lower}(E) = \begin{pmatrix} E - \epsilon_0 & -\alpha & 0 \\ -\alpha & E - \epsilon_0 & 0 \\ 0 & 0 & E - \epsilon_1 \end{pmatrix}^{-1} \tag{16}$$

and find that:

$$G_{12}^{lower} = \frac{\alpha}{(E - \epsilon_0)^2 - \alpha^2} \approx \frac{\alpha}{(E - \epsilon_0)^2}. \tag{17}$$

Where we have used that α is a weak coupling. The calculation for the lower path is equal to that for the two level system of figure 2a and this demonstrates the result of equation 9. Idem for the upper path way we have:

$$G_{12}^{upper} = \frac{\beta^2}{(E - \epsilon_0)^2(E - \epsilon_1) - 2\beta^2} \approx \frac{\beta^2}{(E - \epsilon_0)^2(E - \epsilon_1)} \tag{18}$$

If we now look at the ratio of the two:

$$\frac{G_{12}^{upper}(E)}{G_{12}^{lower}(E)} = \frac{\beta^2(E - \epsilon_1)}{\alpha} \tag{19}$$

we find that for energies $E < \epsilon_1$ the ratio has a negative sign indicating that there is a phase difference of π between the two paths. Adding the contributions of both paths back together gives to leading order:

$$T(E) = \gamma^2 \left| G_{12}^{upper}(E) - G_{12}^{lower}(E) \right|^2. \tag{20}$$

---

[3]For simplicity the imaginary infinitesimal energy $\pm i\eta$ has been left out, as this drops out in the Transmission Function $T(E)$ anyway.

When both paths have an equal contribution to the conduction $G_{12}^{upper}(E) = G_{12}^{lower}(E)$, these paths cancel and the transmission goes to zero, which shows up as the destructive quantum interference in figure 3c.

2.5 Seebeck Coefficient

When there is a thermal difference across a conductor a thermoelectric potential will arise due to the Seebeck effect. The current density J through a conductor, in the case of such a thermal difference, is given by:

$$J = -\sigma \left(\nabla V + S \nabla T \right). \tag{21}$$

In the zero current steady state the Seebeck coefficient S relates the thermal difference with the electrical potential:

$$S = -\frac{\Delta V}{\Delta T}. \tag{22}$$

For a given conductor its thermoelectric properties determine the magnitude of the Seebeck coefficient. In molecular electronics we're interested in determining the electronic properties of single molecules. One potentially powerful way to do this is by relating the Seebeck coefficient to the Transmission function $T(E)$. We will now show how to do this.

As is often the case in condensed matter, all the relevant physics in metals takes place around the Fermi energy. The Sommerfeld expansion is a useful expansion for low temperature ($k_B T << \mu$) degenerate Fermi gases. Starting from the Landauer formula we can do a Sommerfeld ex-

pansion and relate the Seebeck coefficient to the Transmission function[4]:

$$I = \frac{2e}{h} \int_{-\infty}^{\infty} T(E) \left(f_L - f_R \right) \mathrm{d}E \tag{23}$$

$$= \frac{2e}{h} \frac{\pi^2}{6} \left((k_B T_L)^2 - (k_B T_R)^2 \right) T'(E) \Big|_{E=\mu} + \mathcal{O}\left(\left(\frac{k_B T}{\mu} \right)^4 \right) \tag{24}$$

$$\approx \frac{2e}{h} \frac{\pi^2}{6} \left((k_B T + \Delta T)^2 - (k_B T)^2 \right) T'(E) \Big|_{E=\mu} \tag{25}$$

$$= \frac{2e}{h} \frac{\pi^2}{6} \left(2k_B^2 T \Delta T + (k_B \Delta T)^2 \right) T'(E) \Big|_{E=\mu} \tag{26}$$

$$\approx \frac{2e}{h} \frac{\pi^2}{6} \left(2k_B^2 T \Delta T \right) T'(E) \Big|_{E=\mu}. \tag{27}$$

Since $I = G\Delta V = \frac{2e^2}{h} T(\epsilon_F) \Delta V$, under the assumption that T(E) changes slowly around the Fermi energy. The Seebeck coefficient is:

$$S = -\frac{\Delta V}{\Delta T} = \frac{\pi^2 k_B^2}{3e} T \frac{T'(\mu)}{T(\mu)} \tag{28}$$

$$= \frac{\pi^2 k_B^2}{3e} T \frac{\partial \ln \left(T(E) \right)}{\partial E} \Big|_{E=\mu}. \tag{29}$$

Hence, measuring the Seebeck coefficient for a molecular conductor gives us the derivative of the logarithm of the Transmission function $T(E)$. Representing the broadening of the energy levels ϵ_i of both the HOMO and LUMO by a Lorentzian, as in equation 6:

$$T(E) = \sum_{i=1}^{2} \frac{\Gamma^2}{\left(E - \epsilon_i \right)^2 + \Gamma^2/4}, \tag{30}$$

we get a Transmission function $T(E)$ that looks like the green graph in figure 4. Calculating the Seebeck coefficients according to equation 29 for this Transmission function, we get the blue graph in the same figure. We can see here that the sign of the Seebeck coefficient can be both positive and negative. For a n-type conductor, such as the electrons in the LUMO, the Seebeck coefficient is negative and it is positive for a p-type conductor,

---

[4]Temperature in the context of this text is usually something that is applied or fixed externally, so to avoid confusion I denote a temperature as just a T or ΔT for a temperature difference, while the Transmission function $T(E)$ will always be denoted as some function of energy E or μ.

like the electrons in the HOMO. The resulting potential is schematically shown for a regular conductor in figure 5. The sign of the Seebeck coefficient can tell us if the HOMO or LUMO of the molecule is closer to the Fermi energy.

Because the value of the Seebeck coefficient is dependent only on the derivative of the Transmission function $T(E)$ at the Fermi energy, measuring the Seebeck coefficient only tells us something about the Transmission function $T(E)$ at the Fermi energy. By shifting the chemical potential μ to different energies it is possible to overcome this limitation and measure the Transmission Function $T(E)$ everywhere. This shifting could be done by applying a gating potential perpendicular to the bias potential.
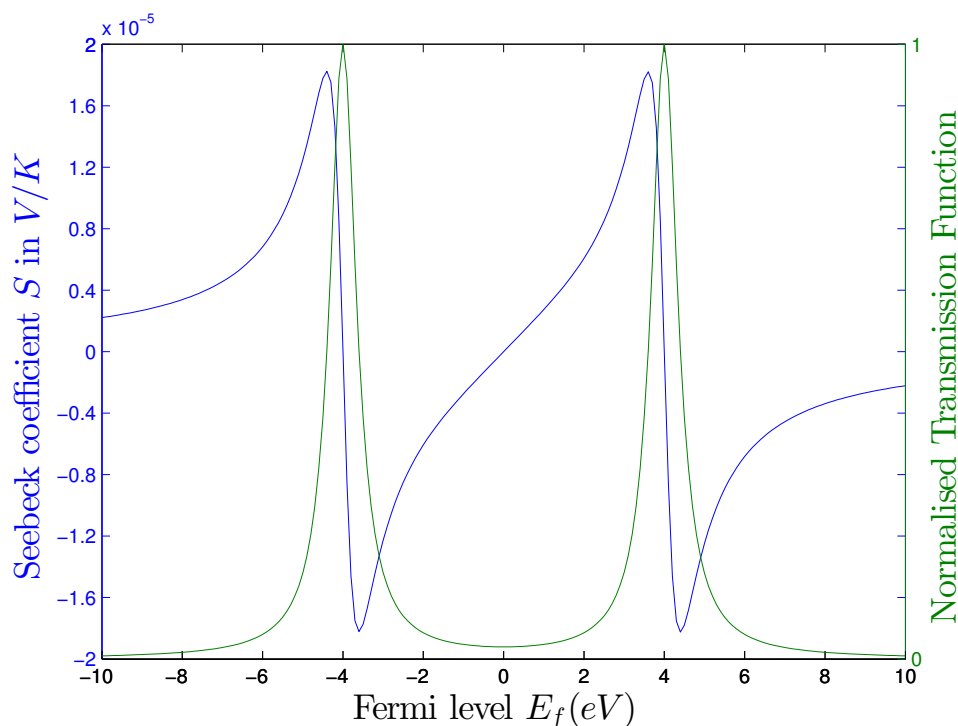
Figure 4: *The green graph shows the Transmission function $T(E)$ for a Lorentzian HOMO and LUMO. While the blue graph shows the corresponding Seebeck coefficient as a function of the Fermi level.*
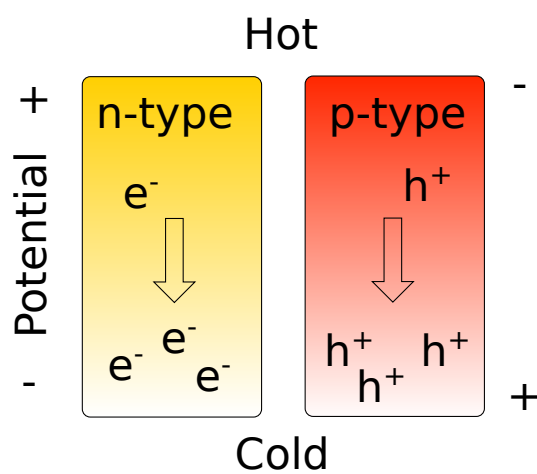
Figure 5: *Depending on the type of conductor the Seebeck coefficient can be positive or negative.*

3   Conductive Atomic Force Microscopy (C-AFM)

The use of an Atomic Force Microscope (AFM) allows us to locally measure the thermoelectric properties of a molecular junction with nanometer resolution, while independently providing feedback for the position of the AFM-tip at the same time. This gives it an advantage over the use of a scanning tunneling microscope (STM), which uses its current sensing for feedback. In this section we will detail the operations of an AFM and show some of the conductance measurements that can be made with Conductive Atomic Force Microscopy. We will discuss the feasibility of measuring the Seebeck coefficient by applying a temperature difference. We will then consider how an existing AFM setup could be modified to allow for thermopower measurements.

3.1   Atomic Force Microscopy (AFM)
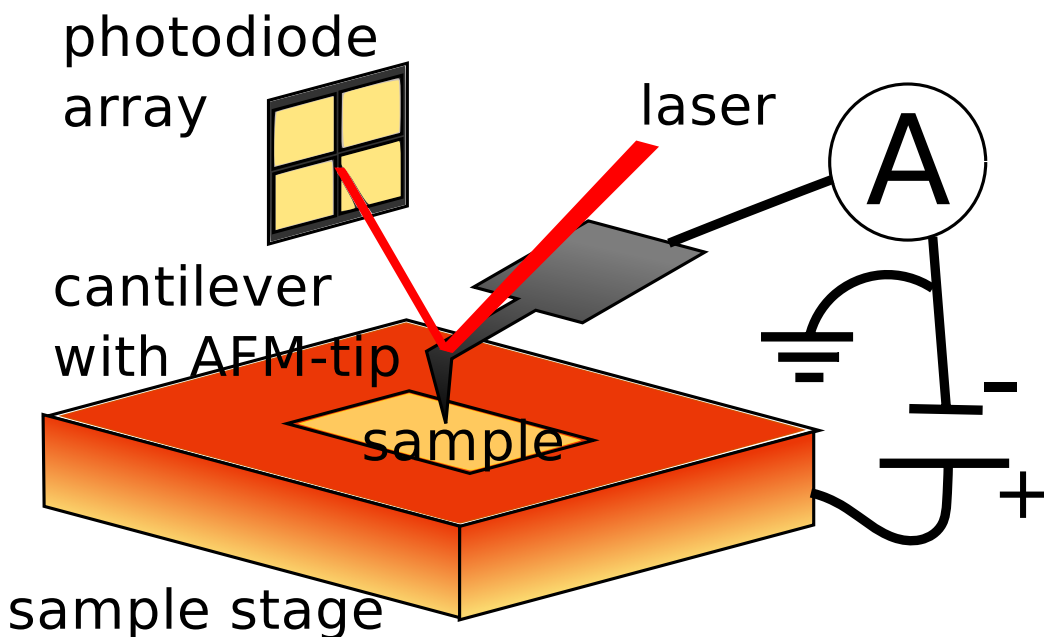
Figure 6: *Overview of the AFM-setup. When the AFM-tip is in contact with the sample the cantilever bends. This deflects the laser beam reflecting of the back of the cantilever. The deflection is then measured by the photodiode array.*

Atomic Force Microscopy (AFM) uses a small tip on a cantilever to scan the surface of a sample. The tip is placed at the end of the cantilever so that

when the tip is brought into close proximity to the surface of the sample, the cantilever deflects due to the forces between the tip and the sample (see also figure 6). This deflection is commonly measured by reflecting a beam of laser light of the back of the cantilever. The reflection of the beam is aimed at the middle of a photodiode array. When the cantilever bends, the position of the beam on the photodiode shifts away from the centre. This signal is then used to map the topography and provide feedback to keep the probe at a constant height above the sample.

3.2 AFM tip

Resolutions of a fraction of several nanometre are possible with an AFM. The resolution of an AFM is limited by the radius of the tip at the contact point, thus sharpness is extremely important. Tip radii of several nanometers can be reliably manufactured. The geometry of a tip can be conical, but is most commonly a pyramid, as they are produced by growing a crystalline structure.
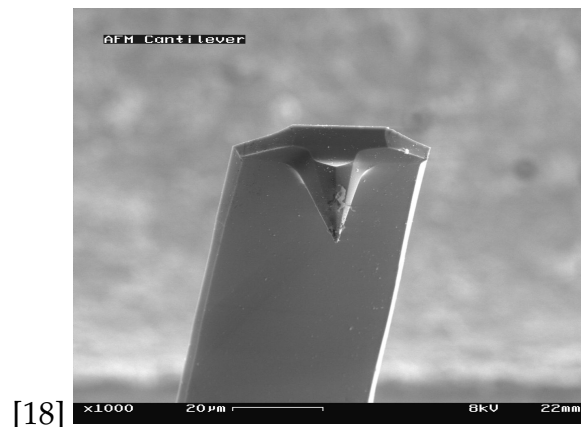
[18] ![figure]

Figure 7: *A Scanning Electron Microscopy image of a typical AFM tip and cantilever.*

3.3 C-AFM measurement setup

In addition to providing the relief of the surface, a special type of AFM can also map the conductive topography of the sample by using a conductive probe. For Conductive Atomic Force Microscopy (C-AFM) the deflection of the beam provides feedback to keep the probe in contact with the surface at a constant force. While at the same time the local electric properties

of the sample can be measured through the probe. The local conductance of the sample can be measured by applying a small bias voltage to the sample and measuring the corresponding current as is the case in Scanning Tunneling Microscopy (STM). In traditional STM the feedback is provided by this current, while the benefit of C-AFM is that the feedback is generated separately from the conductive measurements, by the deflection of the laser signal. Still, it is often possible for a C-AFM to use the current for feedback and operate in a STM-like mode.

3.4 Conductive measurements

Conductive Atomic Force Microscopy (C-AFM) can be used to measure the current, due to an applied bias, through a Self Assembled Monolayer (SAM). This produces IV-curves that can often yield a lot of information about the electronic properties of such a SAM. As an example we will look at some results from H. Ateşçi and V. Kaliginedi[19]. The Ruthenium complexes shown in figure 8c and 8d have phosphonic-acid groups at the top and bottom, which enables them to bind covalently to an Indium Tin Oxide (ITO) substrate and form a monolayer. By adding Zirconium-ions to the solution, after a layer has formed, it is even possible to start the development of a new layer. In this manner the molecules can be stacked in several layers. These stacks could be used to build stable molecular devices from the bottom-up. Using a gold coated tip, C-AFM was used to study the properties of two types of Ruthenium complexes, usually referred to as Ru-C and Ru-N.

The two molecules are almost completely identical, except for the ligand group of atoms in the middle. In the case of the molecule in figure 8c, the middle group is a benzene-like ring. Here the two carbon atoms that are coordinated with the Rubidium atoms are highlighted. In the molecule of figure 8d these carbon atoms have been replaced by nitrogen atoms.

These differing atoms result in different IV-curves as can be seen in figures 8b and 8a. In the left figure applying a positive bias of $1V$ to Ru-C yields a current of up to $0.05nA$, while a negative bias of $-1V$ yields $-0.1nA$ at $\pm 1V$. For the Ru-N complex on the right the overall current is a factor of 4 higher. Unlike the first molecule, it also attains the higher current of $0.4nA$ at positive bias. While the causes behind this difference are quite difficult to explain due to the complexity of the molecules and are still under study, it does show that small changes in the chemistry of a molecule can have significant effects on the electronic transport properties, it also shows that very clear results can be attained with C-AFM.

Thus C-AFM is a very potent technique to probe the properties of self assembled monolayers. The addition of thermopower measurements can make it even more powerful, as we will see in the following section.

3.5 Feasibility of Seebeck measurement

The Seebeck coefficient for molecular junctions can be quite high, especially when the molecule exhibits destructive quantum interference. For AQ-DT molecules this can be as high as $\pm 2 mV/K$[3], which is about three orders of magnitude higher than the Seebeck coefficient S of most common metals at $\pm 1 \mu V/K$[22]. The thermopotential U scales with the temperature difference ΔT over the conductor. Molecular junctions, such as those made by a self-assembled monolayer, are only nanometers in thickness, thus it requires a large thermal gradient ∇T between the cold and hot reservoir, for there to be a significant temperature difference ΔT across the junction. This severely limits the range of the temperature difference ΔT for which we can measure the thermoelectric properties of the junction. Although most of this report is about what a realistic temperature difference ΔT over a molecular junction would be, we assume for the moment that 10 Kelvin is doable. At a temperature difference of 10 Kelvin there could be a signal of up to $U = 20mV$ for a junction with the quantum interference exhibiting molecule AQ-DT. This DC signal is well within the measurable range of electronic voltmeters.

To measure the thermoelectric potential U over a conductor it is necessary to connect electrodes to the material. This means that if there is a temperature difference ΔT across the material, for which we wish to determine the Seebeck coefficient S, there will also be a temperature difference over the electrodes. Thus the electrothermal potential at the far end of the electrodes will be a sum of the potential over the molecular junction and of the thermoelectric potential caused in the rest of the measuring setup. This introduces a systematic error. When the Seebeck coefficient S for the molecular junction is much larger than that of the electrodes, it could be justified to not account for this error. For junctions with lower Seebeck coefficients it might be necessary to compensate for this error source. Another type of systematic error is caused by contact potentials, which arise when two different metals are in electrical contact. While the Fermi energies in both metals will be equal, a potential will still arise between the two metals, due to the difference in Work functions of the metals. Contact potentials are independent of temperature and only contribute a static potential, thus do not change when varying the temperature and can thus be

(a) IV-curve of Ru-C

(b) IV-curve of Ru-N

(c) Chemical structure of Ru-C

(d) Chemical structure of Ru-N
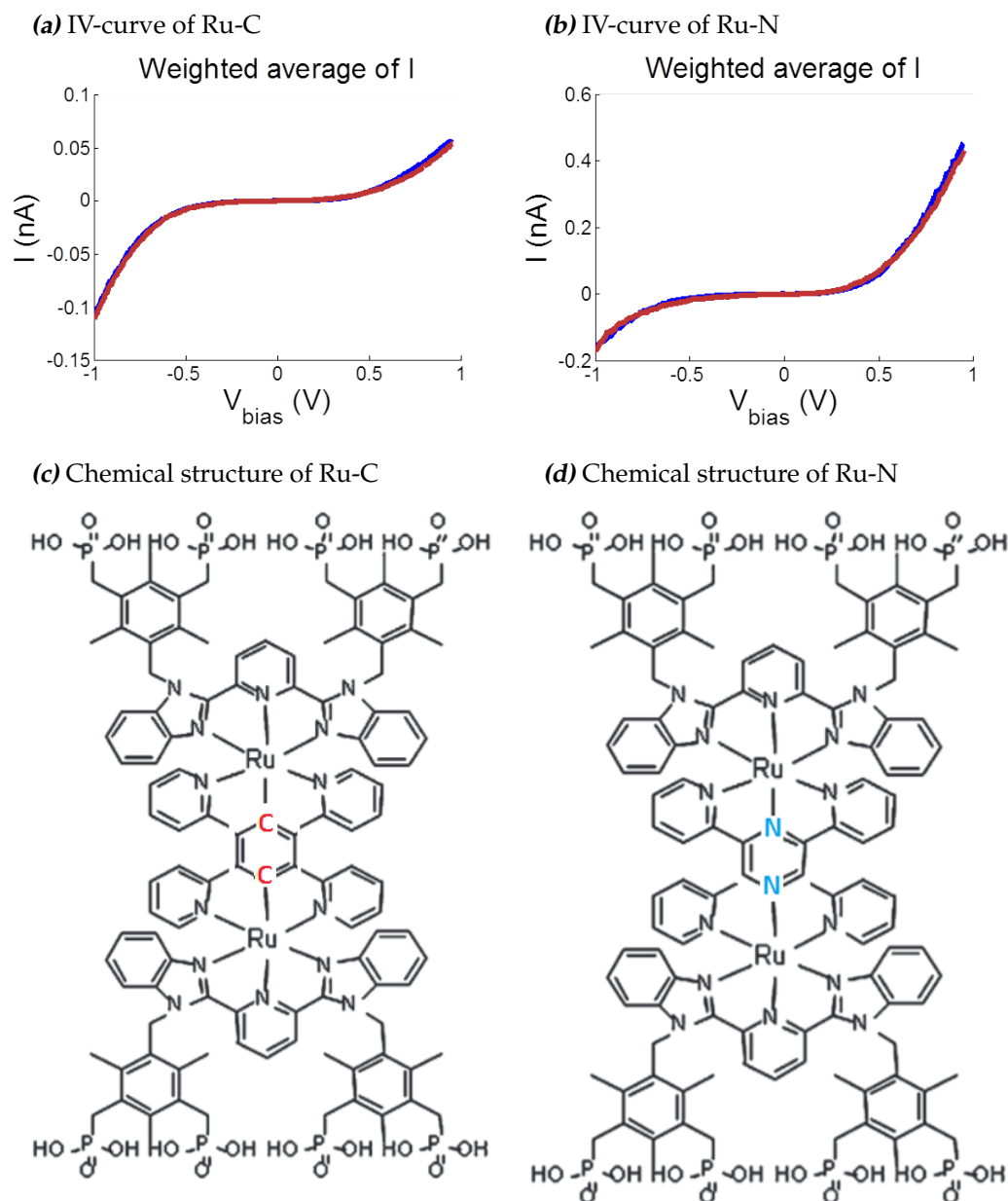
Figure 8: *Current-potential measurements taken with a gold coated C-AFM tip (a and b) of two different Ruthenium complexes (c and d). While the molecules only differ in the substitution of two carbon atoms by nitrogen atoms, their IV-spectra are quite different. Results were obtained under Nitrogen atmosphere by H. Ateşçi and V. Kaliginedi[19]. Molecules are synthesized in the group of M. Haga[20] and images 8c and 8d are taken from [21]*

calibrated out.

In a perfect measuring setup it would be possible to know how the heat is distributed along the measuring path. By using the Seebeck coefficients of the materials in this path it would be entirely possible to calculate the resulting thermoelectric potential and correct for it. Atomic Force Microscopy is a technique to image the properties of a material on a nanometer scale. This requires that the AFM-tip is also the size of several nanometers. This poses a problem as thermal conductance is low at such dimensions, which makes it difficult to control the distribution of heat in the measurement setup. An additional problem is that the dimensions and thus conductive properties of an AFM-tip not only vary from tip to tip, but due to wear, also change during use. This makes it difficult to account for any thermoelectric potential over the AFM-tip.

If it is necessary to compensate for the systematic error in the thermoelectric potential, then the potential over the AFM-tip must be made as small as possible. This means that the temperature gradient needs to occur elsewhere in the system and the tip should be at a uniform temperature. The only way to guarantee this is if the thermal conductance of the AFM-tip is high relative to the thermal conductance of the self assembled monolayer (SAM). When the base of the AFM-tip is then in close proximity to a heat reservoir of known temperature[5], the entire AFM-tip will then be at the same temperature, as it looses only a small amount of heat through the more insulating SAM. The desired temperature distribution is schematically shown in figure 9.

At sample preparation the self assembled monolayer is usually formed on a metal substrate, commonly gold. The metal substrate is thermally well conducting and because it is spread out has a large thermal capacitance. Thus it is unlikely that the substrate will cause an error in the thermal potential.

In the situation described above it is possible to compensate for the systematic error in the thermoelectric potential. To do this, we need to know the temperature of the AFM-tip, the temperature of the substrate and the ambient temperature of the measuring apparatus[6]. By connecting the reservoir of the AFM-tip and the substrate to the voltmeter, at ambient temperature, with wires with a known Seebeck coefficient, it is possible to calculate the resulting thermoelectric potential. The open-voltage ther-

---

[5]The reservoir can be also a heat source or sink, but the important thing is that the heat capacity is sufficient for the whole thing to have a well defined temperature.

[6]Technically it is only necessary to know two temperatures if we assume that either the substrate or the AFM-tip are already at ambient temperature.
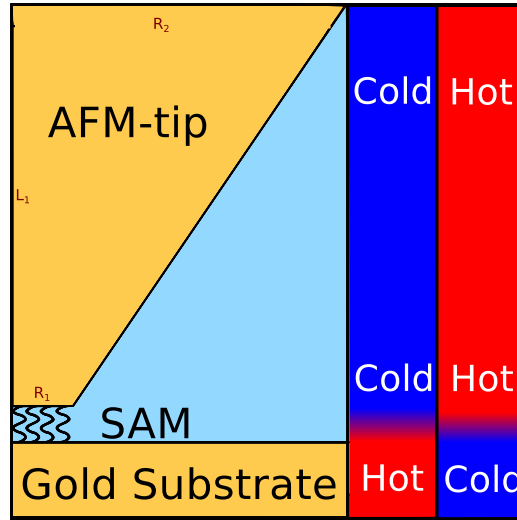
Figure 9: *To prevent any systematic measurement errors, a temperature profile as shown on the right in the figure is desired. The entire AFM-tip can be either cold or hot, but should have a uniform temperature and any temperature gradient should occur over the molecular layer denoted SAM.*

mopotentials that need to be corrected will then simply be given by:

$$\Delta V_A = -S_{wire}(T_1 - T_3) \tag{31}$$
$$\Delta V_S = -S_{wire}(T_2 - T_3) \tag{32}$$

Here $\Delta V_{A,S}$ are the potentials over the wires connected to the AFM-tip and the Substrate. Temperature T_1 is the temperature of the reservoir of the AFM-tip and T_2 is the temperature of the substrate, while T_3 is the ambient temperature[7]. For accurate measurement, wires with a consistent Seebeck coefficient are needed, thus wires that are used to make thermocouples would be recommended, since these are produced to exhibit a predictable thermoelectric effect.

3.6 Practical design considerations

The main focus of this report is on the general difficulties faced when measuring thermoelectric properties at the nanometer scale. There are however some practical challenges related to the use of Atomic Force Microscopy for this purpose. In this section these problems and pointers to possible solutions will be outlined. Some commercially available AFM's

---

[7]These numbers are consistent with the choices made in figure 12a

can with little modifications be used for C-AFM type measurements. Most of them, however, are not set up for thermopower type measurements. Thus when trying to equip an existing AFM with these capabilities, some issues arise. Most of which are space constrains related.

In order to measure the Seebeck coefficient of a material, a temperature difference is required. Thus the AFM setup needs to be modified to include a way to heat or cool part of the sample locally in a controlled manner. For the purpose of measuring the thermopower of a self assembled monolayer, there are two obvious places to do this: either include a heater at the bottom of the sample holder or incorporate the heater into the design of the AFM-tip and tip holder.

A typical AFM places the sample on a motorized and piezo controlled stage that moves the sample into contact with the AFM-tip. The range of this stage is unfortunately limited. Depending on the model, the stage can only be lowered by about 1 centimeter. Thus if we wish to mount a heater or cooler beneath the sample, the design can only be a couple of millimeters high. This precludes placing a Peltier element directly below the sample to cool it. It would be possible to cool the sample stage by connecting it with a thermally conductive (copper) mesh wire to an external cold reservoir, except that the sample stage is vibrationally isolated from the rest of the AFM and the connection to an external reservoir with a too heavy lint wire could carry vibrations. Therefore I believe that the best solution to heat the sample would be to run a simple wire heater under the sample. As heating such a small sample does not require a lot of power and the wires can be kept thin and flexible.

Applying heat (or cold) directly to the tip of the AFM does not introduce any extra vibrations to the sample stage, but poses a bigger engineering challenge. Building a wire heater directly into an AFM tip could be a very good solution, but this requires fabricating custom AFM-tips with nanotechnology. This is too complex for this report, so we will not explore this much further.

Connecting the AFM-tip to a hot or cold reservoir is a more feasible solution. To measure thermoelectric properties with an AFM, the AFM-tip needs to be electrically conductive and connected to a volt or source meter. Preferably this electrical path should be electrically isolated from the rest of the AFM measuring setup. The AFM-tip however should not be thermally isolated, as the AFM-tip and electrical leads alone have an insufficient thermal capacity, which makes temperature control and stability difficult. I would therefore recommend using the entire AFM-tip holder as a heat reservoir, by constructing it out of metal and designing it in a way that the electrical path from the AFM-tip is isolated, but still

thermally conductive. This can be accomplished for example by using aluminium(III) oxide as an insulating material. Although other materials can be used if these facilitate fabrication.

To measure a Seebeck coefficient only a temperature difference needs to be applied and except for the sign it does not matter if the bottom of the sample is hot or the AFM-tip. There are some issues to consider when measuring the thermoelectric properties of molecular junctions. Self assembled monolayers can be quite stable at room temperatures [23], but degrade at higher temperatures. Thus when heating above room temperature it is better to keep the sample at room temperature and heat the AFM tip.

To prevent degradation of the molecular junction it is better to use cooling techniques to establish a temperature difference. When done under atmospheric conditions condensation will occur. Unfortunately this already occurs in small amounts at room temperature and increases in severity when approaching the freezing point. While in liquid form the presence of a layer of condensation will contribute to the conductance and influence the measurements of the thermoelectric properties. When frozen it could destroy the sample and make any measurement impossible. It is therefore advisable to do these kind of experiments under vacuum. When such a setup is not available, it might be possible to use a sealed chamber around the AFM and flush it with nitrogen to reduce the humidity. Such a technique was also used for the results in figure 8. When combined with cooling techniques a cold trap could be used to eliminate most of the remaining humidity and enable measurements under atmospheric pressure below the freezing point. In this case it is better to heat the bottom of the sample instead, to make sure that any initial condensation does not happen on the sample.

In conclusion there are several options available to do thermopower type measurements with an existing AFM setup. But some consideration should be given to the desired temperature difference and range. As these decisions determine the required design for the AFM-setup. Here the choice is between simply heating the sample or tip or more elaborately cooling the setup with the advantage of a larger temperature range and more stability for the molecular junction.

In this chapter we have mostly discussed the design considerations for the AFM-setup and how we can practically cool or heat the sample. Whether or not it is possible to create such a temperature gradient over a nanometre thick Self Assembled Monolayer (SAM) is still unclear. In the next chapter we model the AFM-tip and sample in COMSOL and try to answer this question.

4 Comsol simulations

Determining the thermoelectric properties of molecular junctions can be very useful to characterize the molecular transport properties. Among other things, it enables us to measure the derivative of the logarithm of the Transmission Function $T(E)$ at the Fermi energy. All thermoelectric effects involve temperature gradients and one method of measuring the Seebeck coefficient is to apply a temperature difference to both sides of a molecular device. However, for the extremely small length scales of these devices it is questionable if any significant temperature difference can exist between two points that are very close together. Yet in order to determine the thermoelectric properties of these devices a large temperature difference is required to yield a usable signal. To accurately measure these properties we need to know what the actual temperature difference is that we are applying over the device, in case some of the thermal potential falls over some other part of the measuring set-up. We also need to know if such a temperature difference can be maintained.

To answer these questions we have used the commercial finite elements program Comsol. Simulations were made of an AFM tip in contact with a self assembled layer monolayer (SAM) of the molecular conductor on a gold substrate. Comsol was in particular used to determine the dominant heat transfer process: conduction, convection or radiation and under which physical parameters these phenomenon are dominant. Comsol was also used to determine the effect of several parameters on the magnitude of a temperature difference across the molecular layer. These parameters include the dimensions of the AFM tip and the thermal resistivity of the SAM.

4.1 A 1-D model

A first description of heat transfer through the AFM tip and SAM is a simple 1-D model, which is informative because it represents a situation with only conductive heat transport, showing how the temperature difference changes when we include convection and radiation. In this simulation we assume that there are three linear elements. The simulation is outlined below:

Simulation elements:

- The AFM-tip made of a material with thermal resistance R_{tip}, for the Comsol simulation it is assumed that the tip is made of solid 1-D
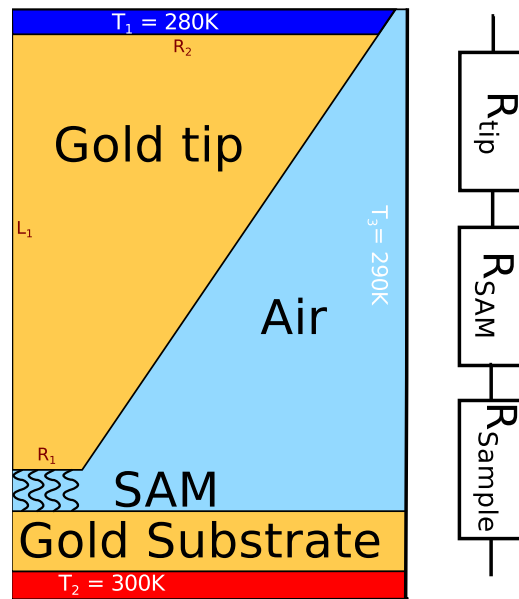
Figure 10: *The thermal elements in the Measuring setup, as shown on the left, can for the purpose of calculating the heat transport be replaced with equivalent 1-dimensional thermal resistances, as shown on the right.*

gold. It is assumed that the tip has a length of 100nm.

- The SAM layer with thermal resistance value of R_{SAM}. We want to determine the required value for this parameter, that allows us to generate a large enough thermal potential. This value is therefore varied.

- The gold-substrate with a length of 100nm.

Boundary Conditions:

- The top op the tip is fixed at $T_1 = 280K$

- The bottom of the substrate is fixed at $T_2 = 300K$

- It is assumed that there is no heat loss via the 'sides' of this 1-D conductor.

Material properties:

Gold:

- Thermal Conductivity $k = 320W/mK$

- Density $\rho = 19300 kg/m^3$

- Heat capacity at constant pressure $C_p = 129 J/kgK$

The thickness of a typical self assembled molecular layer is in the order of ten nanometer. This is six orders of magnitudes smaller than the dimensions of the substrate and the AFM-tip, it is therefore not very enlightening to subdivide this element in more finite elements. In this simulation we simulate the SAM by using a Comsol boundary condition called Thin Thermal Resistive Layer, this condition introduces a discontinuity in the model, which is determined by:

$$-n_d \cdot (-k_d \nabla T_d) \;=\; -\frac{T_u - T_d}{R_s} \tag{33}$$

$$-n_u \cdot (-k_u \nabla T_u) \;=\; -\frac{T_d - T_u}{R_s} \tag{34}$$

$$\text{with } R_s \;=\; \frac{d_s}{k_s} \tag{35}$$

here k_s is the thermal conductivity and d_s the thickness of the layer, u and d denote the top and bottom of the layer.

Results

(a) without self assembled monolayer **(b)** with self assembled monolayer
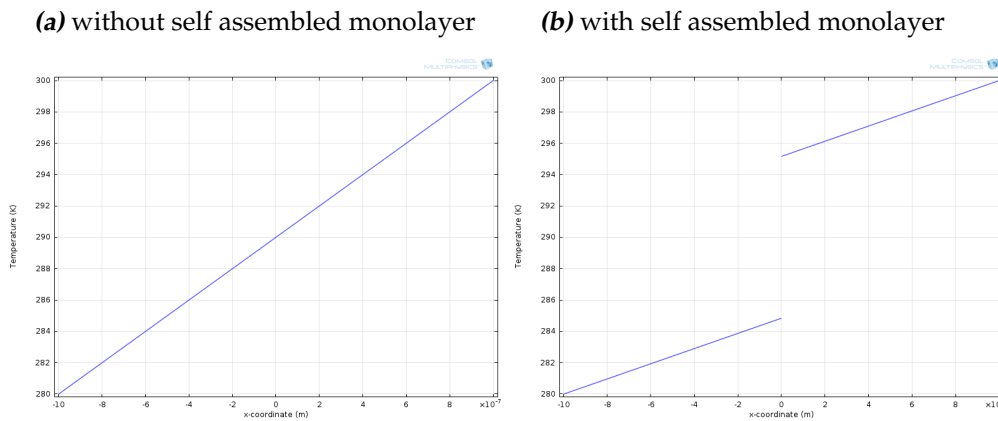
Figure 11: *The 1-D Comsol simulation without a SAM in (a) shows a straight line for the temperature corresponding to the constant thermal resistivity in the two gold elements. Introducing a very thin SAM with a low thermal conductance of $k_{SAM} = 1.5 \cdot 10^{-8} W/K$ (b) causes a discontinuity in the temperature at the boundary where the SAM is present.*

The problem of finding the distribution of heat in a device is similar to finding how the potential drops in an electrical circuit, as such we can expect three different thermal resistances over which the temperature gradient will be linear. To test if our simulation works as expected and that the Thin Thermal Resistive Layer option does what it is supposed to, we first run this simulation with this option off. The result is shown in figure 11a. This simulation is little more than two pieces of hundred nanometre long 1-D gold attached together and the result is a constant thermal gradient over the 200 nanometres, where the temperature varies from 280K at the top and 300K at the substrate. This is what we expect analytically if we have a simple resistance model, as in figure 10, with the resistance of R_{SAM} equal to zero.

When the Thin Thermal Resistive Layer is turned on, a discontinuity is introduced where the tip and substrate meet, this translates into a jump in the temperature in the results of figure 11b. The size of this jump is determined by the value of the thermal resistance of the SAM R_{SAM} via equations 33-35.

As the 1-D model is simply a model of three conductive elements in series, it does not include any convective or radiative heat transfer. If conduction is the dominant heat transfer process that determines the magnitude of the temperature difference over the SAM, then the 1-D model is a good approximation to predict this difference. For a particular measuring setup, which has a fixed material and geometry for the AFM-tip, the only variable of interest is the value of the thermal resistance of the SAM R_{SAM}. In order to have a temperature difference remaining of approximately $10K$, when applying a temperature difference of 300K-280K=20K, a thermal conductance value for the monolayer of $1.5 \cdot 10^{-8} W/K$ is needed as can be seen in figure 11b. Assuming a thickness for the monolayer of 10 nanometre, this corresponds to a conductivity k of $1.5 W/mK$. We will later compare the 2-D situation to this value.

4.2   Heat transfer in a radial 2-D model

To include convection and radiation in the heat transport calculations we need more than one dimension. If we assume that our AFM-tip is conical, then the entire problem can be made axially symmetric, which makes it possible to represent the results in 2-D. Comsol was used for a finite elements simulation of this axially symmetric problem. In figure 12a the simulated AFM-tip and sample set-up is visualised to give a quick overview of the geometry and the boundary conditions that were used and will be
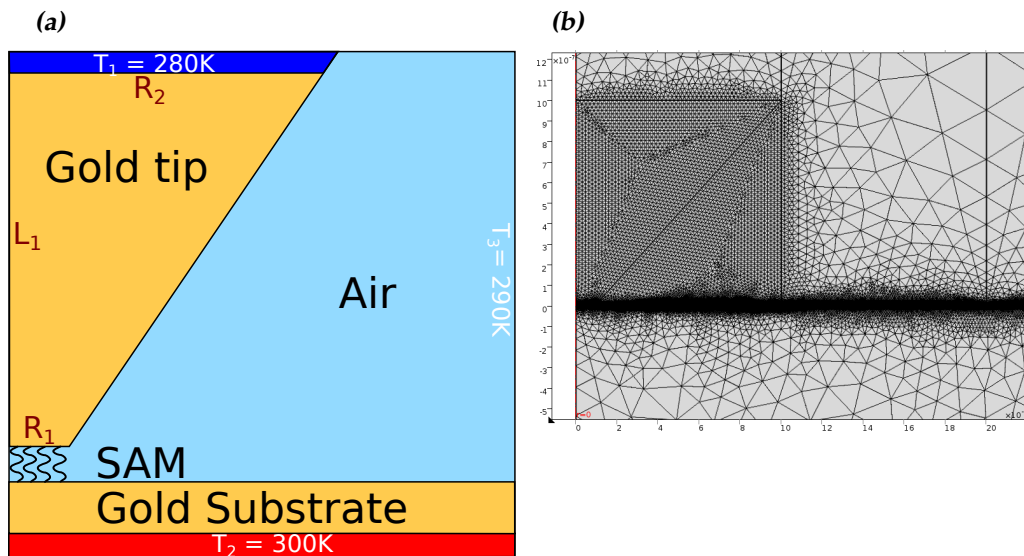
Figure 12: *The simulated 2-D model of an AFM setup. (a) Schematic overview of a radially symmetric AFM-tip with the simulated elements: AFM-tip, gas, SAM and gold substrate with the relevant boundary conditions for the temperature.(b)The mesh that is used in the Comsol simulation. It is locally scaled to the dimensions of the elements.*

outlined below.

Simulation elements:

- The AFM-tip is modelled with a conical element and has a fixed length denoted by L_1 of $10^{-6}m$, its radius at the bottom and top are given by R_1 and R_2 respectively. These radii were varied, but have a default value of $R_1 = 10^{-7}m$ and $R_2 = 10^{-6}m$. The bottom of the tip is in contact with the the self assembled monolayer (SAM).

- The sample substrate is simulated by a cylindrical element with a height of $10^{-5}m$ and a radius of $3 \cdot 10^{-5}m$. These dimensions were not varied.

- The surrounding gas consists of a connected square and triangular element, which fill all the space between the tip and the sample. The block of gas has dimensions of $10^{-5}m$ by $2.9 \cdot 10^{-5}m$.

- Between the gold substrate and the AFM-tip is a very thin element

representing the self assembled monolayer (SAM)[8]. This element has a thickness of only ten nanometers and covers the surface of the substrate. The finite element mesh was adjusted to this small scale by setting the maximum element size to one nanometer, as can be seen in figure 12b.

Boundary conditions:

- The entire problem is axially symmetric and the entire simulation is therefore done in 2D in Comsol the left boundary has an axially symmetric boundary condition to account for the mirror symmetry.

- The bottom and right most boundary of the gold sample is fixed at temperature $T_1 = 300K$.

- A fixed temperature $T_2 = 280K$ at the top of the AFM-tip.

- The edges of the gas element are fixed at a temperature T_3, which in some simulations is equal to T_1 or T_2 but sometimes in between at 290K. This value has an insignificant effect on the results.

Material properties:

Gold:

- Thermal Conductivity $k = 320W/Km$

- Density $\rho = 19300kg/m^3$

- Heat capacity at constant pressure $C_p = 129J/kgK$

- To test radiative transport an emissivity ϵ of 0.5 was used.

SAM:

- The thermal conductivity of the SAM was varied from $k = 320W/mK$ to $k = 2 \cdot 10^{-5}W/mK$.

- The values for density $\rho = 19300kg/m^3$ is set equal to that of gold.

---

[8]In earlier simulations the SAM was represented by the Thin Thermally Resistive Layer as in the 1-D simulation. However, this option proved unreliable for the 2-D simulation, therefore the SAM was represented by an object with very small element dimensions.

- Heat capacity at constant pressure $C_p = 129 J/kgK$ is set equal to that of gold.

- To test radiative transport an emissivity ϵ of 0.5 was used.

gas:

- Ratio of specific heats $\gamma = 1.4$[9]

- The default values from the Comsol materials database were used for the heat capacity at constant pressure, density, thermal conductivity, electrical conductivity and speed of sound.

4.3   Dependence of the thermal resistance on the geometry

The magnitude of the temperature difference over the self assembled monolayer (SAM) depends on the relative difference in thermal resistance between the gold AFM-tip and the SAM. In one dimension the only way to change the thermal resistance of a piece of gold is by increasing the length. In two dimensions the thermal resistance between the top of the AFM-tip and the bottom of the tip also depends on its shape or geometry. To explore this dependence and at the same time become familiar with the model, we will vary the size of the radius of the contact area with the SAM R_1 and vary the size of the base or top of the AFM-tip R_2. Both these variations affect the amount of gold there is to conduct heat and therefore change the thermal resistance of the AFM-tip.

Changing the radius R_1 at the bottom of the tip affects the 'sharpness' of the AFM-tip and a very small radius R_1 means that there is only a small part of the AFM-tip in contact with the SAM, while a very large R_1 corresponds to a blunt tip and a large contact area. Thus varying the radius R_1 has two effects. With increasing radius the thermal resistance of the gold decreases, increasing the temperature difference over the SAM, and at the same time the contact area increases, which causes the thermal resistance of the SAM itself to decrease. In figure 13a the result for the variable R_1 is shown. Here R_1 was varied from $20nm$ to the size of R_2 at $1000nm$, in the last case the AFM-tip is completely cylindrical. The figure shows that with increasing R_1 the temperature difference drops, indicating that the thermal resistance drop of the SAM is a larger effect.

---

[9]Although I am certain this value has no effect on the simulation as varying it does not change the results and it does not show up in any of the equations that govern the physics in the simulation. Comsol refuses to run the simulation without this constant, so I have included it for completeness sake.

Increasing the size of R_2 has no effect on the contact area, but only increases the thermal conduction through the gold of the AFM-tip. This can be seen in figure 13b, which shows an increasing temperature difference for an increasing R_2, starting at a small cylinder with the same radius for R_1 and R_2 at $100nm$ till a maximum of $1000nm$.

In these simulations some parameters have been set to values that do not necessarily correspond to those for a real setup. The results for the radii of the AFM-tip, where there is a maximum temperature difference across the SAM, are therefore not automatically the real dimensions for the optimal AFM-tips. This still depends on other variables such as the thermal conductivity of the SAM. In general we can, however, conclude that the thermal resistance of the AFM-tip should be as low as possible. This can be accomplished if the base of the AFM-tip has a sufficient radius and consists of solid gold or other thermally conductive metal. The bottom of the tip should, however, remain sharp and have a small contact area with the SAM in order to limit the thermal transport through the SAM.

4.4   Radiative transport

Gold, like most metals, conducts heat very well with a value of the thermal conductivity of $k = 320W/mK$. Thermal radiation is governed by Stefan-Boltzmann's law $j = \sigma \epsilon T^4$, where σ is Boltzmann's constant and ϵ denotes the emissivity of the grey body. Thus thermal radiation is very weak for low temperatures. If the conduction through the AFM tip is significantly lowered by the thermal resistance of the Self-Assembled Monolayer (SAM), then the contribution of the thermal radiation to the total heat transfer might be important.

To see if radiative thermal transport should be included in the Comsol simulations, a test has been done where there is no conduction through the SAM. This has been accomplished by setting a very low value of $k = 2e^{-5}W/mK$ for the thermal conductivity of the SAM. The simulation has also been done in 'vacuum', by disabling all conduction through the 'gas' parts of the simulation, so this is a comparison between the heat conduction inside the tip and radiative heat transfer from the sample. All surfaces have been set to an emissivity $\epsilon = 0.5$ as the exact values are not very relevant. The 2-D simulation has been extended to include two $1\mu m$ square golden elements that are floating in vacuum, in order to confirm that radiative heat transfer is working in the simulation.

The results for including radiation into the simulation can be seen in figure 14, where the simulation has been done for five different temper-
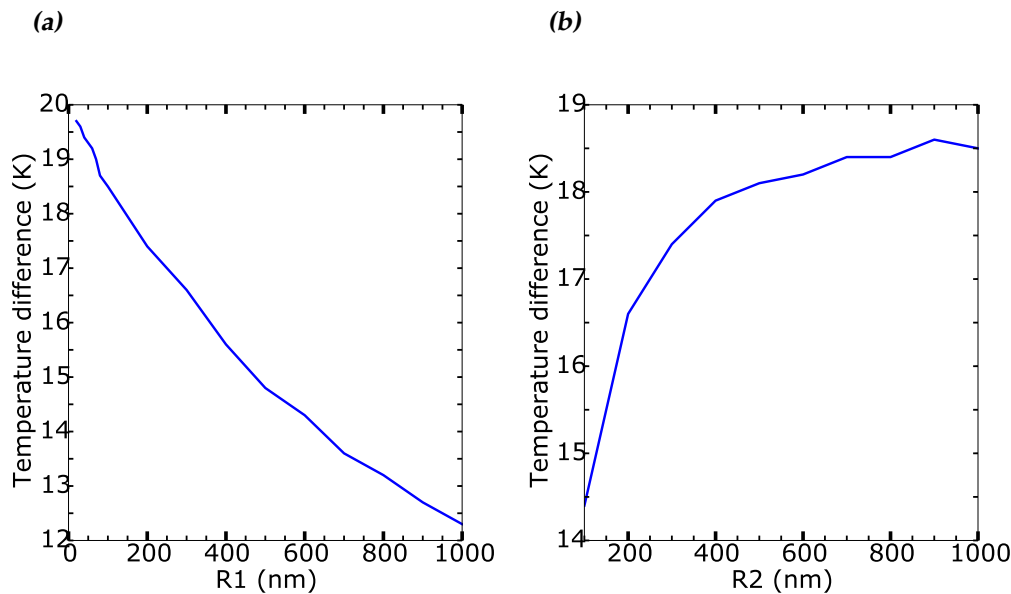
Figure 13: *The effect of variations in the geometry on the temperature difference over the SAM in Kelvin. The total applied temperature difference is 20 Kelvin. (a)Increasing the radius R_1 from $20nm$ to the size of R_2 at $1000nm$ causes the temperature difference to drop, due to an increase in contact area with the SAM.(b) Increasing R_2 from a small cylinder with radius $R_1 = R_2 = 100nm$ to a conic AFM-tip with base $R_2 = 1000nm$ increases the temperature difference over the SAM by increasing the conductance of the AFM-tip.*

atures of the sample at 300K, 500K, 1000K, 10000K and 100000K. In this simulation the top of the AFM tip has been held at a temperature of 280K and is thus connected to an infinitely large heat sink. For the first four temperatures up to 10000K (figures 14a till 14d), we see that the entire AFM tip is cold at a uniform 280K (dark red), even if the sample is heated to a glowing and non-physical ten thousand Kelvin! We can therefore conclude that the conduction inside the gold is significantly stronger than the radiative heat transfer.

To check that the radiative heat transfer in the simulation actually works, we have included two floating gold elements. These elements can only gain or loose heat via radiation, since they are not connected to anything and conduction through the 'vacuum' is disabled. One element is placed at a height of $3\mu m$ above the heated sample and the other is placed at a height of $8\mu m$. Unfortunately Comsol draws the thermal gradients also in vacuum, which is why the entire plot is coloured. However, this has

no real physical meaning, since vacuum has no particle density nor a heat capacity.

The easiest way to see that radiative transport is working to look at figure 14d for the sample temperature $T_2 = 10000K$. Here the test-element at the top is a bright yellow, denoting a temperature of about $7000K$. It acquired this temperature because it is irradiated by the glowing hot sample at 10000K. The effects of including the thermal radiation can be seen in all of the subfigures of figure 14. However, its effects are more subtle. In all figures the elements are heated above their initial temperature of 280K. In all figures the top element is heated above the temperature you would expect from the temperature gradients for conduction alone, so it is not just an artefact in the way Comsol plots the temperature distributions, although again there is not actually a gradient outside of the gold elements. Although both test-elements are almost at the same temperature and loose a similar amount of heat via radiation, the bottom element appears to be lower in temperature than its surroundings, which are not cooled by radiating. Again indicating that radiative transport is working. As a final test the temperature of the sample has been increased to a hundred thousand Kelvin in figure 14e. Here finally the AFM-tip begins heating up due to the massive amounts of thermal radiation, so unless the temperatures are extremely high we can neglect the contribution of radiative heat transport, which is done in all of the following simulations.

(a) 300K

(b) 500K

(c) 1000K
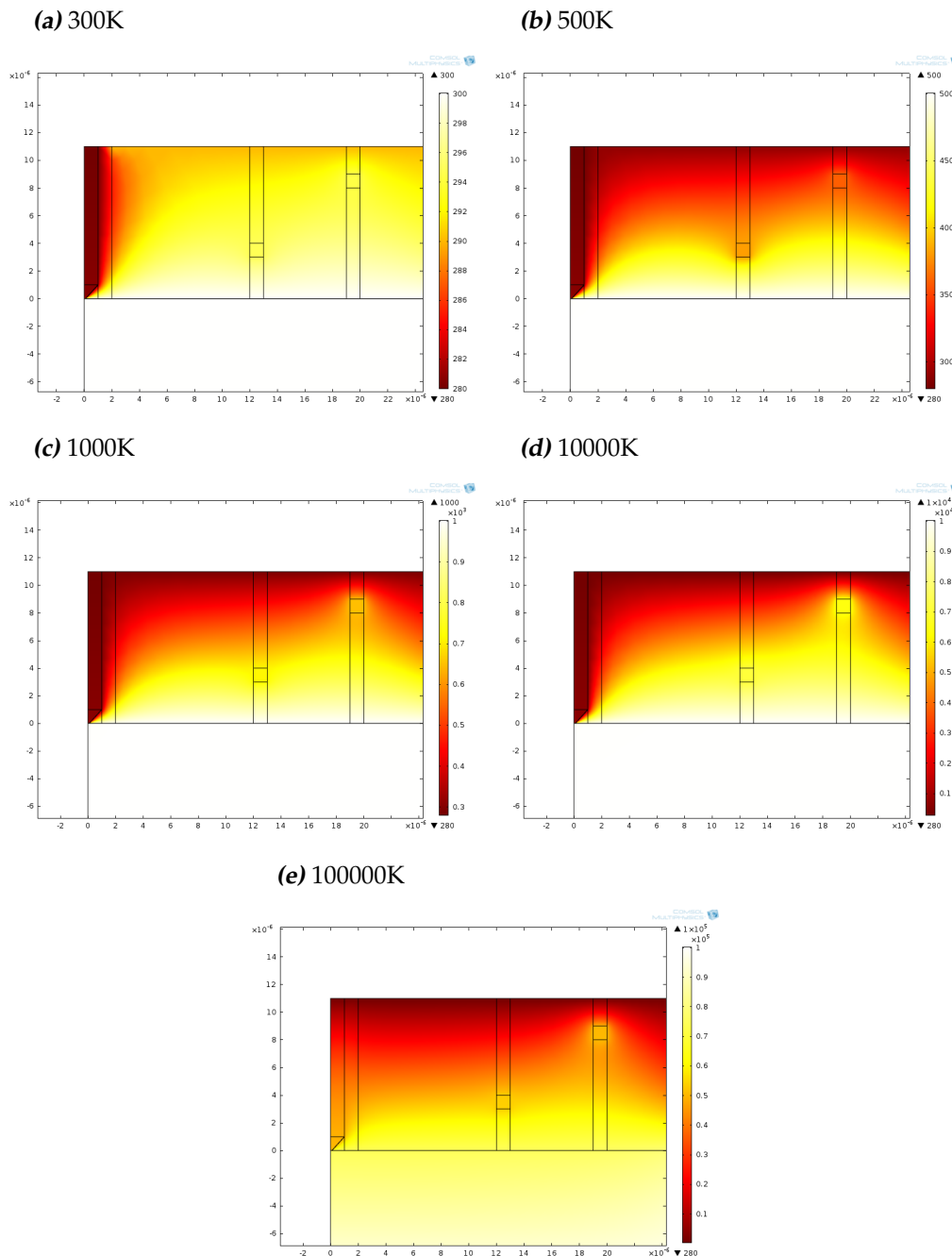
(d) 10000K

(e) 100000K

Figure 14: *To test the effects of radiative heat transport the substrate was heated to temperatures from 300K to 100000K. The AFM-tip (to the left in the figures) stays cool at 280K up to 10000K! At 100000K the AFM-tip is heated up due to the massive amounts of thermal radiation. In all of the figures an extra golden element is included that is not connected to conductive materials to show that radiative heat transport is present.*

4.5 Dependence on molecular thermal resistance

To measure the thermoelectric properties of a molecular layer, a temperature gradient must be applied over it. This is only possible if the thermal resistance of the molecular layer is sufficiently high, otherwise any temperature difference will disappear due to heat transfer. This is what we have assumed till now. By varying the thermal conductivity k of the SAM in the 2-D simulation, we can determine at what values there still is a temperature difference and thus discover what thermal resistance is sufficiently high.

In figure 15a the result of this variation can be seen on a logarithmic plot for k in W/Km. When the SAM has the same conductivity as gold at $k = 320W/Km$, the temperature difference disappears, as is to be expected for a layer of only 10nm in thickness. The temperature difference over the SAM increases with declining conductivity and reaches the full $20K$ at conductivities lower than $0.1W/Km$.

At a value of $k = 10W/Km$ there is a temperature difference of about 10K. This is a realistic value for the temperature difference for a measurable thermoelectric effect, if the molecular layer has a high Seebeck coefficient. The thermal conductivity k should therefore be below $10W/Km$, when using an AFM-tip that has similar dimensions to those of the simulation.

Measured values for the thermal conductance of alkane thiol molecules in a self assembled monolayer are in the range of $30 - 10pW/K$[24] for different numbers of carbon atoms. Figure 15b is taken from the 2014 article of Meier et al[24] in which these measurements are shown. The density of such a SAM has an average number of molecules of $4.7nm^{-2}$[25]. Thus these measured thermal conductances correspond to thermal conductivities of about $k = 0.7W/Km$ with the simulated layer depth of 10nm. This means that the thermal conductivity is low enough to generate a measurable signal, since it is below $10W/Km$, but care should be taken when attributing the temperature drop to the thermal resistance of the SAM as it is above the value of $k = 0.1W/Km$[10] and there could still be a significant temperature gradient across the AFM-tip or measurement set-up itself. Only if the thermal conductivity is several orders of magnitude below this value, the importance of knowing the thermal resistances of the measuring set-up diminishes.

---

[10]Again this value is not actually an absolute number. It all depends on the ratio between the thermal resistance of the measuring set-up and the SAM.

(a)

(b)
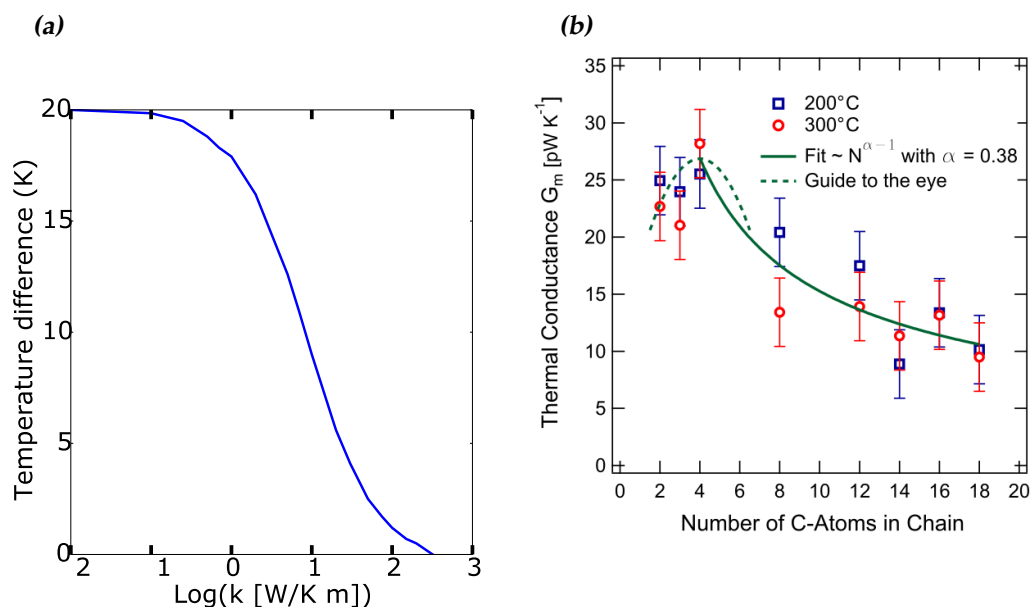
Figure 15: *Thermal resistance of the molecular layer.(a)Varying the thermal conductivity k of the SAM shows that there is a maximum temperature difference for conductivity at $k < 0.1 W/Km$, while the temperature difference disappears completely when the conductivity is set equal to that of gold at $k = 320 W/Km$.(b)Measured values for the conductance of alkane thiol molecules in a SAM with different chain lengths. This figure was taken from the 2014 article by Meier et al[24].*

4.6 Building a 1-D analytical model for the 2-D simulation

From figure 15a it was concluded that for a temperature difference of more than 10K over the SAM we need a thermal conductivity of $k < 10 W/Km$, in the 1-D simulation we found a value for the thermal conductivity of $1.5 W/mK$. This value is an order of magnitude lower than the one we derived from figure 15a. However, in that 2-D model the AFM-tip has a conical shape with a radius of only 100nm at the contact area with the SAM. The results from figure 13a and 13b show that a conical tip has a higher conductance: relative to a straight wire, with radius equal to r_1, it has more conductive material. Thus the SAM can have a higher conductivity and still show a 10 Kelvin temperature difference. This explains the order of magnitude difference between the 1-D and 2-D simulation.

The problem of conductive heat transport through a one dimensional structure is a relatively simple one and can be solved analytically. Two-dimensional or higher problems can be significantly more work to solve

depending on the complexity of the geometry. When the gradient is directed only in a single direction, such problems can be reduced to a one-dimensional problem and can be readily solved again.

Unfortunately this is not entirely true for our 2-D geometry, because the sample is not a simple cylinder of roughly the same dimensions as the AFM-tip and there is thus a discontinuity in the radius when going fromt he sample to the AFM-tip. We can of course pretend that it is and approximate the temperature distribution for the 2-D case when we only take conduction into account. This we can then compare to the more involved calculation done using Comsol.

The 2-D simulation exist of three elements: AFM-tip, SAM and sample (see figure 10), for which we can approximate their thermal resistances in the vertical direction. In this approximation we take both the SAM and the sample to be cylindrical with a radius equal to r_1 and r_3.[11]. The thermal resistance for a cylinder is given by:

$$R = \frac{\rho L}{A} = \frac{\rho L}{\pi r^2}. \tag{36}$$

The thermal resistivity ρ is defined as $1/k$. The AFM-tip itself is a cone for which the thermal resistance is:

$$
\begin{aligned}
R_{cone} &= \rho \int_0^L \frac{1}{\pi \left(r_1 + \frac{r_2 - r_1}{L} y \right)^2} \mathrm{d}y \\
\ldots &= \frac{\rho L}{r_2 - r_1} \frac{1}{\pi} \int_{r_1}^{r_2} \frac{1}{x^2} \mathrm{d}x \\
\ldots &= \frac{\rho L}{\pi} \frac{1}{r_2 - r_1} \left(\frac{1}{r_1} - \frac{1}{r_2} \right) \\
R_{cone} &= \frac{\rho}{\pi} \frac{L}{r_1 r_2}
\end{aligned}
\tag{37}
$$

The total resistance is the sum of the resistances for the SAM, AFM-tip and sample:

$$R_{total} = \frac{\rho_{gold}}{\pi} \left(\frac{L}{r_1 r_2} + \frac{\rho_{SAM}}{\rho_{gold}} \frac{D_{SAM}}{r_1^2} + \frac{D_{sample}}{r_3^2} \right) \tag{38}$$

---

[11]In the Comsol simulation the SAM and the sample are also represented by cylindrical elements. However, there radius is so large in comparison to the AFM-tip that it becomes infinite for the purpose of the simulation.

Here D_{SAM} and D_{sample} are the depths of the layers. The temperature difference over the SAM is then given by:

$$\frac{R_{SAM}}{R_{total}} = \frac{\Delta T}{T_{total}} \tag{39}$$

We can now use this model to compare the 2-D situation with the results from the 1-D COMSOL simulation.
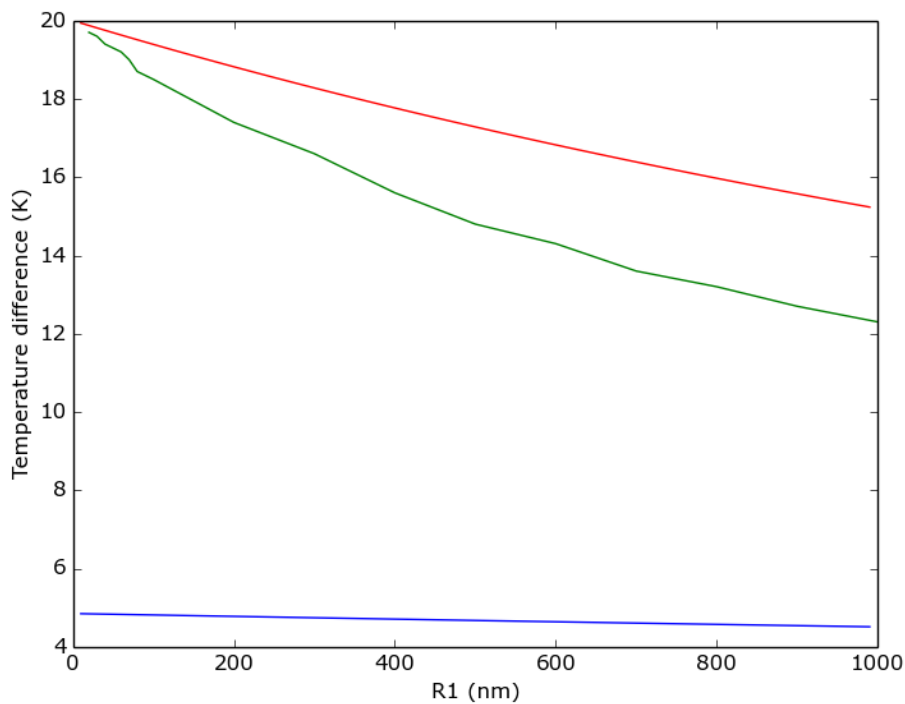
Figure 16: *The green graph shows the result from the 2-D Comsol simulation. As indicated by the blue line, choosing the radius of the sample $r_{sample} = r_1$ in the analytical model, clearly does not correspond to the simulation. Assuming that the substrate has an infinite conductance (shown in red) over estimates the temperature difference, but follows the trend of the simulation quite well.*

4.7   Discussion of Comsol simulations

Using the values that correspond to the simulation we can compare the model of the previous section to the results of figure 13a. This will tell us

if we can approach the 2-D situation as a model with only 1-D equivalent resistances. Due to the jump discontinuity there is some ambiguity in the value for the thermal resistance of the gold sample. Pretending that it is a very narrow cylinder of radius $r_{sample} = r_1$ doesn't work as denoted by the blue line in figure 16. Overestimating its conductance by stating that its radius is infinite, so that its thermal resistance becomes zero, produces the red line in the figure. This line is quite close to the Comsol data and shows the correct behaviour, although it overestimates the temperature difference due to setting the thermal resistance of the substrate to zero completely. This result suggests that our analytical model for 1-D conduction is mostly accurate and that conduction is the only relevant heat transfer process. As only accounting for thermal conduction already shows a good match, it makes it unlikely that convection in the surrounding gas has a large contribution to the thermal conductance. This also means that doing the experiment in vacuum will not help with regards to the magnitude of the temperature difference.

The 1-D and 2-D finite element simulations in Comsol were used to model the temperature difference over a self assembled monolayer (SAM) of the molecular conductor. When we included radiative heat transfer in the 2-D simulations there was only an effect to the temperature of the AFM-tip at extremely high temperatures $T > 10000K$. We can therefore conclude that heat transfer via thermal radiation is negligible compared to heat transferred via thermal conduction. This combined with the result of comparing the 2-D simulation to an analytical model that only includes conduction, brings us to the conclusion that thermal conduction in the AFM-tip and SAM is the dominant heat transfer process, for the physical dimensions corresponding to a set-up with a realistic AFM-tip.

Simulations with varying geometries for the AFM-tip show that the AFM-tip should be large enough to have a good thermal conductivity. A tip made of solid conductive metal is most likely to yield good results. It has also been shown that the bottom of the tip should remain sharp and have a small contact area with the SAM in order to limit thermal transport through the SAM. Careful consideration should be given to the choice of AFM-tip in order to maintain good results over repeated measurements.

Measurement of the value for the thermal conductance of alkane thiols place this value at $10pW/K$ per molecule[24], which corresponds to a conductivity of $k = 0.7W/Km$. If this value is representative for the thermal conductance of other such molecules, then measuring the thermoelectric properties of real molecular junctions is possible, since our simulations show that there is a sufficient temperature difference at values below $k = 10W/Km$ for the modelled AFM-tip. However, the ability to mea-

sure these properties is strongly dependant on the thermal resistance of the measuring set-up, thus this should be well designed and cannot be neglected unless the thermal conductivity of the molecules to be inspected is several orders of magnitude lower. Special care should be taken with molecules that are better conducting than alkane thiols.

5   Summary and outlook

The results in this report show that thermopower measurements on self-assembled monolayers are possible under certain conditions. The Comsol simulations show that a sufficiently large temperature difference develops when the molecular layer is sufficiently thermally insulating ($k < 10W/Km$) and the AFM-tip is sharp enough, so that the contact area between the AFM-tip and SAM is kept to a minimum. Calculations show that it is possible to measure the Seebeck coefficient of molecules displaying destructive quantum interference with a C-AFM setup. Thus conductive probe AFM could be used as a first step to directly show the presence of destructive quantum interference in molecules. The large magnitude Seebeck coefficients that correspond to the strong suppression of the transmission of electrons with a particular energy, makes this a reachable short term target.

It will be challenging to correctly quantify the Seebeck coefficient, due to the possible systematic errors. Thus to move this technique forward it will be necessary to properly design the AFM-measurement setup and to fully characterize it, in order to correct for the thermopotentials that arise within the measuring equipment. Overcoming these issues will enable the accurate measurement of the Seebeck coefficient, the thermal resistivity and other such thermoelectric properties. With finite element simulations in Comsol, we have shown that the temperature difference across a molecular layer is mostly determined by its thermal resistance with respect to the thermal resistance of the measuring setup. It was also found that the dominant heat transfer process is conduction through the AFM-tip and sample. Radiative heat transport and convection through the surrounding gas is insignificant. Thus accounting for all the thermopotentials systems, comes down to accounting for all the thermally conductive elements in the C-AFM setup.

If a mechanism would be discovered to gate the energy levels with respect to the Fermi energy, it would be possible to recover the full Transmission function $T(E)$ of the molecular junction, since the Seebeck coeffient only depends on the Transmission Function $T(E)$ near the Fermi energy. This would thus provide information about the complete electrical properties of the junction, that is not attainable by conventional conductive measurements.

References

[1] S. V. Aradhya and L. Venkataraman, "Single-molecule junctions beyond electronic transport," *Nature nanotechnology*, vol. 8, no. 6, pp. 399–410, 2013.

[2] S. J. van der Molen and P. Liljeroth, "Charge transport through molecular switches," *Journal of Physics: Condensed Matter*, vol. 22, no. 13, p. 133001, 2010.

[3] C. M. Guédon, *Relating orbital structures to the conductance properties*. PhD thesis, Leiden University, 2012.

[4] V. B. Engelkes, J. M. Beebe, and C. D. Frisbie, "Length-dependent transport in molecular junctions based on sams of alkanethiols and alkanedithiols: Effect of metal work function and applied bias on tunneling efficiency and contact resistance," *Journal of the American Chemical Society*, vol. 126, no. 43, pp. 14287–14296, 2004.

[5] https://www.comsol.com/.

[6] D. Fracasso, H. Valkenier, J. C. Hummelen, G. C. Solomon, and R. C. Chiechi, "Evidence for quantum interference in sams of arylethynylene thiolates in tunneling junctions with eutectic ga–in (egain) top-contacts," *Journal of the American Chemical Society*, vol. 133, no. 24, pp. 9556–9563, 2011.

[7] V. Kaliginedi, P. Moreno-García, H. Valkenier, W. Hong, V. M. García-Suarez, P. Buiter, J. L. Otten, J. C. Hummelen, C. J. Lambert, and T. Wandlowski, "Correlations between molecular structure and single-junction conductance: a case study with oligo (phenylene-ethynylene)-type wires," *Journal of the American Chemical Society*, vol. 134, no. 11, pp. 5262–5275, 2012.

[8] J. C. Cuevas and E. Scheer, *Molecular Electronics - An Introduction to Theory and Experiment*. World Scientific, 2010.

47

[9] R. Landauer, "Spatial variation of currents and fields due to localized scatterers in metallic conduction," *IBM Journal of Research and Development*, vol. 1, no. 3, pp. 223–231, 1957.

[10] J. R. Hook and H. E. Hall, *Solid State Physics*. John Wiley & Sons, second ed., 1991.

[11] Y. Imry, "Physics of mesoscopic systems: Directions in condensed matter physics, edited by g. grinstein and g. mazenco," 1986.

[12] B. v. Wees, H. v. Houten, C. Beenakker, J. Williamson, L. Kouwenhoven, M. D. van der., and C. Foxon, "Quantized conductance of point contacts in a two-dimensional electron gas," *Physical Review Letters*, vol. 60, pp. 848–850, 1988.

[13] M. Büttiker, Y. Imry, R. Landauer, and S. Pinhas, "Generalized many-channel conductance formula with application to small rings," *Phys. Rev. B*, vol. 31, p. 62076215, May 1985.

[14] M. Paulsson and S. Datta, "Thermoelectric effect in molecular electronics," *Physical Review B*, vol. 67, no. 24, p. 241403, 2003.

[15] J. M. Thijssen and H. Van der Zant, "Charge transport and single-electron effects in nanoscale systems," *physica status solidi (b)*, vol. 245, no. 8, pp. 1455–1470, 2008.

[16] S. Datta, *Electron Transport in Mesoscopic Systems*. Cambridge University Press, 1995.

[17] C. M. Guédon, H. Valkenier, T. Markussen, K. S. Thygesen, J. C. Hummelen, and S. J. van der Molen, "Observation of quantum interference in molecular charge transport," *Nature nanotechnology*, vol. 7, no. 5, pp. 305–309, 2012.

[18] SecretDisc.   `https://commons.wikimedia.org/wiki/File:` `AFM_(used)_cantilever_in_Scanning_Electron_Microscope,` `_magnification_1000x.JPG`. CC-BY-SA-3.0.

[19] H. Ateşçi and V. Kaliginedi, *Unpublished*.

[20] M. Haga. `http://www.chem.chuo-u.ac.jp/~iimc/english/index.html`.

[21] K.-i. Terada, H. Nakamura, K. Kanaizuka, M.-a. Haga, Y. Asai, and T. Ishida, "Long-range electron transport of ruthenium-centered multilayer films via a stepping-stone mechanism," *ACS nano*, vol. 6, no. 3, pp. 1988–1999, 2012.

[22] C. J. M. Lasance, "The seebeck coefficient." `http://www.electronics-cooling.com/2006/11/the-seebeck-coefficient/`, November 2006.

[23] N. Prathima, M. Harini, N. Rai, R. Chandrashekara, K. Ayappa, S. Sampath, and S. Biswas, "Thermal study of accumulation of conformational disorders in the self-assembled monolayers of c8 and c18 alkanethiols on the au (111) surface," *Langmuir*, vol. 21, no. 6, pp. 2364–2374, 2005.

[24] T. Meier, F. Menges, P. Nirmalraj, H. Hölscher, H. Riel, and B. Gotsmann, "Length-dependent thermal transport along molecular chains," *Physical review letters*, vol. 113, no. 6, p. 060801, 2014.

[25] J. C. Love, L. A. Estroff, J. K. Kriebel, R. G. Nuzzo, and G. M. Whitesides, "Self-assembled monolayers of thiolates on metals as a form of nanotechnology," *Chemical reviews*, vol. 105, no. 4, pp. 1103–1170, 2005.